Modelling Simul. Mater. Sci. Eng. **18** (2010) 034006 (17pp) doi:10.1088/0965-0393/18/3/034006

Discrete dislocation simulations of the flattening of nanoimprinted surfaces

Yunhe Zhang[1], **Erik Van der Giessen**[2] **and Lucia Nicola**[1]

[1] Department of Materials Science and Engineering, Delft University of Technology, 2628 CD Delft, The Netherlands
[2] Zernike Institute for Advanced Materials, University of Groningen, 9747 AG Groningen, The Netherlands

Received 22 October 2009, in final form 1 March 2010
Published 23 March 2010
Online at stacks.iop.org/MSMSE/18/034006

Abstract

Simulations of rough surface flattening are performed on thin metal films whose roughness is created by nanoimprinting flat single crystals. The imprinting is carried out by means of a rigid template with equal flat contacts at varying spacing. The imprinted surfaces are subsequently flattened by a rigid platen, while the change of roughness and surface profile is computed. Attention is focused mainly on comparing the response of the film surfaces with those of identical films cleared of the dislocations and residual stresses left by the imprinting process. The aim of these studies is to understand to what extent the loading history affects deformation and roughness during flattening. The limiting cases of sticking and frictionless contact between rough surface and platen are analyzed. Results show that when the asperities are flattened such that the contact area is up to about one third of the surface area, the loading history strongly affects the flattening. Specifically, the presence of initial dislocations facilitates the squeezing of asperities independently of the friction conditions of the contact. For larger contact areas, the initial conditions affect only sticking contacts, while frictionless contacts lead to a homogeneous flattening of the asperities due to yield of the metal film. In all cases studied the final surface profile obtained after flattening has little to no resemblance to the original imprinted surface.

(Some figures in this article are in colour only in the electronic version)

1. Introduction

Surface roughness plays a crucial role during metal forming processes, since it controls the friction properties until the moment that possibly all asperities are flattened. Deformation of the asperities depends on their distribution, height and on their plastic properties.

Models of rough surface contact have shown that surfaces cannot be just treated as a collection of single asperities and that the choice of the description of surface roughness is critical. So far rough surfaces have been mainly described either as statistical [1, 2] or fractal [3–6], but recent models, e.g. [7], derive their rough surface profile description directly from experimentally measured surfaces.

The evaluation of rough surface profiles has been made possible in the past years by a variety of new experimental techniques, including atomic force microscopy, phase shifting interferometry and laser confocal scanning microscopy. Meanwhile, significant numerical effort has been devoted to artificially reproduce two or three-dimensional rough surfaces that have realistic characteristics, e.g. [8–10].

But how relevant is the precise topography of the surface in the prediction of rough surface evolution under contact loading? To what extent would current models profit by such an accurate description?

The aim of this paper is to investigate, by numerical simulations, whether the plastic behavior of a surface is uniquely determined by its profile or if it is affected by the loading history that has created the profile. To this end, numerical simulations are performed in which first surface roughness is created by nanoimprinting, and subsequently the rough surface is flattened by contact with a rigid platen.

The numerical procedure follows the discrete dislocation plasticity method by Van der Giessen and Needleman [11], that allows for a size dependent treatment of plastic deformation of (sub)micrometer scale asperities, through the computation of the collective motion of discrete dislocations. In order to create a rough surface, single crystal metal thin films are imprinted by an array of equally spaced rigid indenters. Surfaces with different roughnesses are obtained by changing the template profile, specifically the spacing between indenters. The rough surfaces thus obtained are then flattened by a rigid platen, and the results are compared with those for films with the same surface profile but cleared from the loading history, i.e. dislocation- and stress-free at the beginning of compression. In principle, this could be achieved experimentally by heat treatment. The presence of an initial dislocation structure may either facilitate or obstruct the flattening of the surface. Our results reveal that the presence of dislocations in the subsurface region significantly influences the subsequent deformation process.

2. Imprinting

2.1. Model

The metal to be imprinted is idealized as an infinitely long single crystal, which is constrained to deform in plane strain perpendicular to the x_1–x_2 plane (see figure 1). The crystal is assumed to be in the form of a thin film, with thickness h so that the elastic displacement during indentation is small compared with what it would be in a bulky metal specimen; this allows for larger retained imprints at the same indentation depth. The film is elastically isotropic, with Young's modulus E and Poisson's ratio ν. Plastic flow occurs in the crystal as a result of the nucleation and motion of edge dislocations that glide along three sets of slip systems as indicated in figure 1. The Burgers vector of the dislocations has magnitude b, and direction parallel to the slip plane. The line direction of the dislocations is perpendicular to the plane of deformation, consistently with the assumption of plane strain.

The film is imprinted by an infinitely long rigid template with a rectangular wave profile. Each flat contact has length a and the center-to-center spacing between contacts is w. Dislocations are assumed to nucleate from Frank–Read sources in the metal; surface

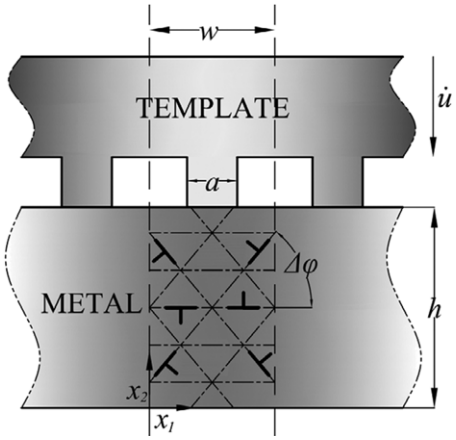

Figure 1. Two-dimensional model of a metal single crystal imprinted by a rigid template with a rectangular wave profile. The width of the contacts is a and the center-to-center contact spacing is w. Calculations are carried out for a unit cell of width w, unless otherwise specified.

nucleation from dislocation steps is not accounted for. The distribution of dislocation sources and obstacles is taken to be periodic in the x_1-direction with period w and the calculations are carried out for a unit cell that lies between $0 < x_1 < w$. The metal is taken to have the elastic properties of aluminum: Young's modulus $E = 70\,\text{GPa}$ and a Poisson's ratio $\nu = 0.33$. There are three potentially active slip systems in the 2D crystal [12, 13], with discrete slip planes oriented at $\varphi = 0^\circ$, 60° and 120° (see figure 1) and spaced at $173b$. The magnitude of the Burgers vector is taken to be $b = 0.25\,\text{nm}$. Initially, the crystal is dislocation free. However, it contains a density $\rho = 30\,\mu\text{m}^{-2}$ of obstacles and of dislocation sources distributed randomly on the slip planes in the crystal. The mean nucleation strength is given as $\bar{\tau}_{\text{nuc}} = 50\,\text{MPa}$ with a standard deviation of 10 MPa for a Gaussian distribution, and the time t_{nuc} for nucleation is taken to be 0.1 ns.

Nucleation from point sources occurs when the resolved shear stress on the source exceeds its critical strength, τ_{nuc} for a given time span t_{nuc}. After nucleation, the glide velocity v^I of the Ith dislocation is proportional to the Peach–Koehler force f^I according to

$$f^I = Bv^I, \tag{1}$$

with B the drag coefficient. Two nearby dislocations with opposite Burgers vector are taken to annihilate when they are within a distance $L_{\text{ann}}6b$. Obstacles to dislocation motion are modeled as points on the slip planes and stop dislocations that attempt to pass through them. An obstacle releases a pinned dislocation when the Peach–Koehler force on the dislocation exceeds $\tau_{\text{obs}}b$, where the obstacle strength is here taken to be $\tau_{\text{obs}} = 150\,\text{MPa}$.

2.1.1. Boundary conditions. The loading is imposed by prescribing normal displacement under the contacts

$$u_2(x_1, h) = -\int \dot{u}\,\mathrm{d}t, \qquad \frac{w}{2} - \frac{a}{2} \leqslant x_1 \leqslant \frac{w}{2} + \frac{a}{2}. \tag{2}$$

We assume that the contact between metal and indenters be perfectly sticking. Thus, the lateral displacement on the contact surface satisfies

$$u_1(x_1, h) = 0, \qquad \frac{w}{2} - \frac{a}{2} \leqslant x_1 \leqslant \frac{w}{2} + \frac{a}{2}. \tag{3}$$

The traction distribution along the contact determines the imprinting force F (per unit of out-of-plane length):

$$F := -\int_{w/2-a/2}^{w/2+a/2} \sigma_{22}\,\mathrm{d}x_1.$$

Outside the contact region, the top surface ($x_2 = h$) is traction free, which requires

$$\sigma_{12}(x_1, h) = \sigma_{22}(x_1, h) = 0, \qquad 0 < x_1 < \frac{w}{2} - \frac{a}{2} \quad \text{and} \quad \frac{w}{2} + \frac{a}{2} < x_1 < w. \tag{4}$$

The boundary conditions along the bottom of the unit cell, $x_2 = 0$, are taken to be

$$u_2(x_1, 0) = 0 \qquad \sigma_{12}(x_1, 0) = 0. \tag{5}$$

Periodic boundary conditions are imposed on the sides of the simulation cell by requiring

$$u_1(w, x_2) - u_1(0, x_2) = 0 \qquad u_2(0, x_2) = u_2(w, x_2), \tag{6}$$

thereby incorporating the lateral constraint imposed by the rigid, sticking indenters.

Even though the computations assume small strains, the contact between the rigid template and the film is based on the deformed film surface. The calculation is performed incrementally. At each time step, the stress and deformation state is determined using superposition of a singular field and an image field solution [11]. The singular field is associated with the discrete dislocations and is calculated analytically. The image field is obtained from the finite element solution of the associated non-singular linear elastic boundary value problem. Once the stresses have been determined, the incremental change in position of each dislocation is calculated, and conditions are checked for nucleation, annihilation of dipoles and pinning at or release from obstacles. Details on the numerical procedure for solving the governing field equations and constitutive equations are presented in [14].

2.2. Imprinting simulations

Thin films are imprinted by rigid templates with different spacings between indenters in order to obtain surfaces with various roughness. Simulations are performed for contacts whose center-to-center spacing w ranges from 1 to 10 μm. The contact width of each indenter is $a = 0.1\,\mu$m and the film height is $h = 2\,\mu$m. The films are imprinted to a maximum depth of $u_{\max} = 0.05\,\mu$m with an indentation speed of $\dot{u} = 4 \times 10^4\,\mu\mathrm{m\,s^{-1}}$. The films are then unloaded at the same speed and subsequently allowed to relax.

The imprinting force for various w is plotted in figure 2(a). When the template contacts are closely spaced (small w) a larger force is required to imprint the films. This is partly due to the different elastic stress states developing during loading, but mainly to a different plastic behavior: the plastic zones underneath closely spaced contacts interact with each other and give rise to a harder response (see also [14, 15]). Figures 3(a)–(c) show the stress σ_{22} and dislocation distribution in the unit cells for $w = 2$, 5 and 10 μm at the maximum imprinting depth ($u = 0.05\,\mu$m). The dislocations mainly distribute underneath the indenter in the central region of the unit cell. The plastic region is isolated from neighboring contacts in the film with largest spacing between indenters, but when contacts are close to each other as in the case $w = 1\,\mu$m the plastic zones interact and cause a harder response (see figure 2(a)). For the simulations just shown the center-to-center contact spacing w corresponds to the unit cell width. It is reasonable to suspect that the different plastic responses for different w could be attributed to the different sizes in the unit cell and therefore related to the boundary conditions imposed on the unit cell. To investigate this issue we perform a simulation in which the center-to-center contact spacing is $w = 2\,\mu$m and the unit cell width is $5w = 10\,\mu$m, therefore comprising five contacts. A larger unit cell with more contacts has the additional advantage

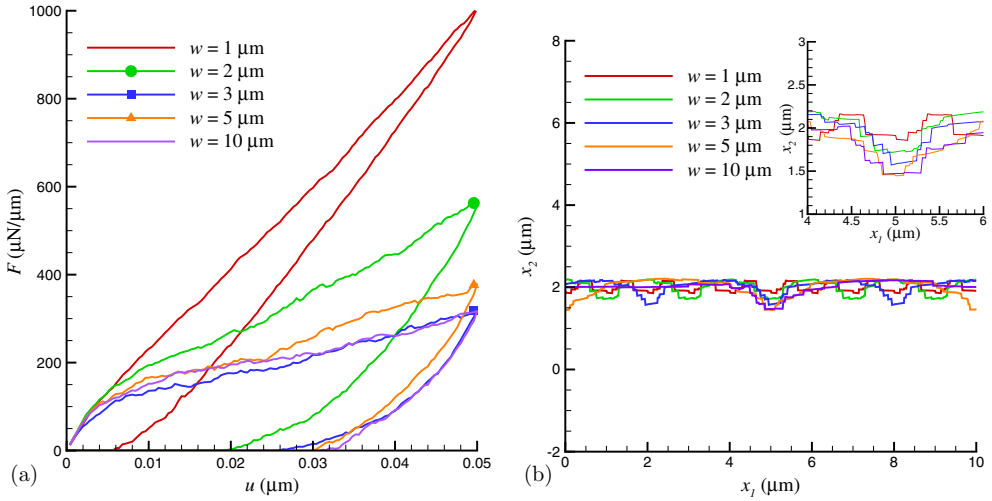

Figure 2. (*a*) Force response during imprinting with contacts of $a = 0.1\,\mu$m for values of the spacing w from 1 to $10\,\mu$m. (*b*) Profile of the top surface after unloading and relaxation for the various templates (i.e. different spacings between indenters). The maximum imprinting depth is $u_{\max} = 0.05\,\mu$m. The vertical displacements of the top surface are magnified by a factor 20 for ease of visualization.

that statistical effects, related to the sampled source distribution, are reduced. The stress state for this simulation is presented in figure 3(*d*). A comparison between figures 3(*a*), (*d*) and (*c*) shows that there is no artifact due to boundary conditions in case (*a*) and confirms that hardening in cases (*a*) and (*d*) is indeed caused by interactions between plastic zones.

In the loaded state, the surface profile seen in figure 3 clearly exhibits imprints that are significantly wider than the contact size $a = 0.1\,\mu$m. Also, there is some finer roughness that has accumulated from the slip steps created when dislocations left the material through the free surface. Upon unloading, the induced dislocation structure dissolves partially but even after relaxation a dislocation structure remains. The final roughness of the surface, comprising the remnant imprints and nearby material pile-ups, is shown in figure 2(*b*), where the vertical displacements are magnified by a factor 20 for ease of visualization. We choose to describe the roughness of the obtained surface profiles by means of the root-mean-square surface roughness R_{m}, defined as

$$R_{\mathrm{m}} = \sqrt{\frac{1}{N}\sum_{i=1}^{N}(h_i - h_{\mathrm{m}})^2}, \tag{7}$$

where N is the total number of top surface nodes, h_i is the vertical coordinate of node i and h_{m} is the mean surface height as well as the height–height correlation function, $H_{\mathrm{r}}(r)$, defined as

$$H_{\mathrm{r}}(r) = \frac{1}{N}\sum_{i=1}^{N}\left[(h(x_1(i)+r) - h_i)\right]^2, \tag{8}$$

where $0 < r < w$; $x_1(i)$ is the x_1-coordinate of the ith node and $h(x_1(i))$ is its height ($=h_i$). This correlation gives insight into the sharpness of the surface roughness.

Figure 4 shows the evolution of the roughness R_{m} during nanoimprinting, unloading and relaxation and the height–height correlation functions at $t = 3\,\mu$s. The general trend seen in figure 4(*a*) is that the roughness at maximum load increases with decreasing w. The film

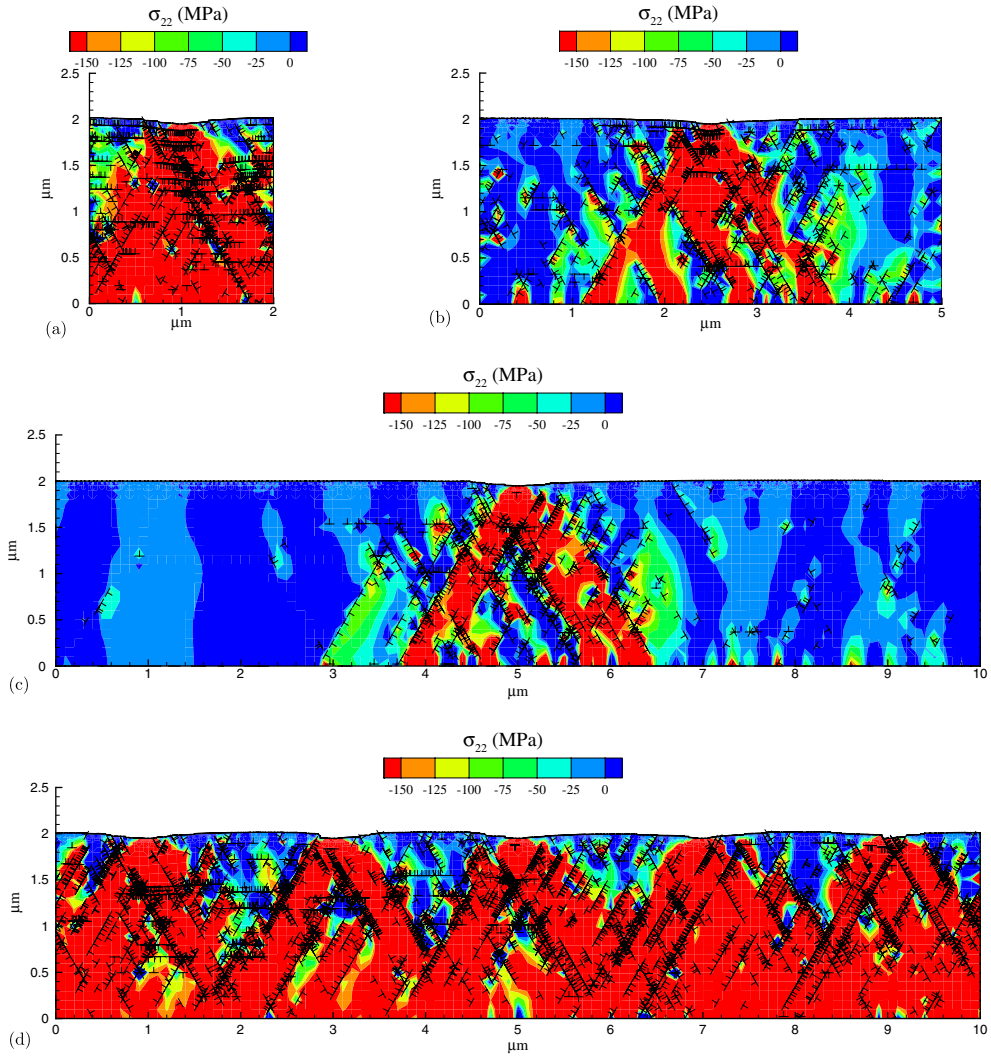

Figure 3. The stress distribution at the maximum imprinting depth $u = 0.05\,\mu$m for (*a*) $a/w = 0.1/2$, (*b*) $a/w = 0.1/5$ and (*c*) $a/w = 0.1/10$ and (*d*) $5 \times a/5w = 5 \times 0.1/10$.

with $w = 1\,\mu$m is an exception in that the elastic spring back is larger than for the other cases (see also figure 2) due to a very strong interaction between plastic zones. The height–height correlation functions after relaxation in figure 4(*a*) show a bimodal behavior: when contacts are closer together than $w = 7\,\mu$m, the curve has a single peak, while two peaks are typical for more spaced contacts. The single peak signifies that the roughness increases with the wavelength, i.e. there is a distinct central imprint with material being piled up at the borders of the unit cell. In other words, the shape of the final surface resembles a wave that has the same periodicity as the spacing between indenters w (see also figure 3(*d*)). For films with $w > 5\,\mu$m the largest material pile-up is not located centrally between contacts but closer to the imprint.

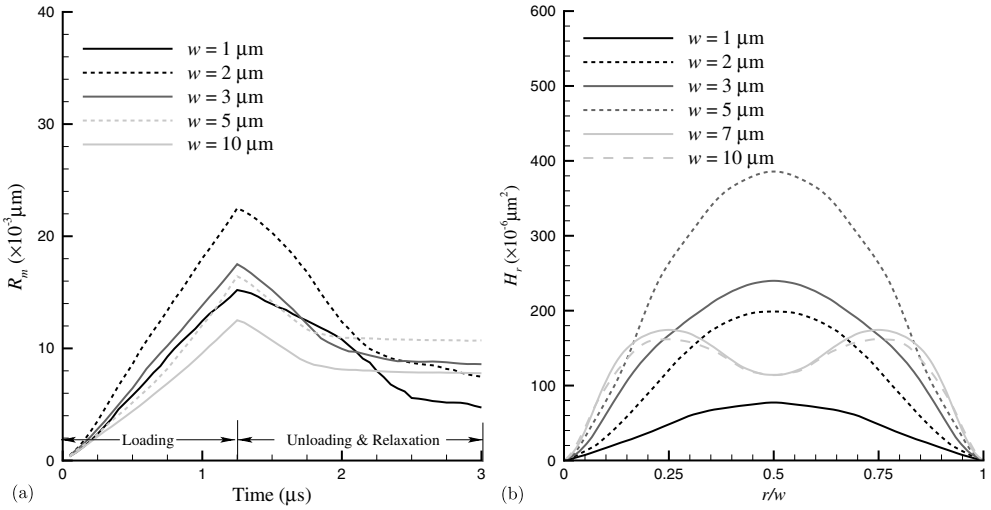

Figure 4. (*a*) Roughness R_m during imprinting, unloading and relaxation. (*b*) Height–height correlation functions $H_\mathrm{r}(r)$ at $t = 3\,\mu$s for films with various values of w, namely $w = 1\,\mu$m, $w = 2\,\mu$m, $w = 3\,\mu$m, $w = 5\,\mu$m and $w = 10\,\mu$m.

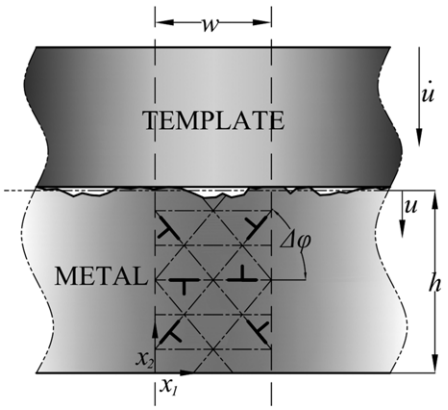

Figure 5. Two-dimensional model of a metal single crystal compressed by a rigid flat platen. The unit cell has the same width w as in the imprinting simulations.

3. Flattening of the rough surfaces

In this section the rough surfaces obtained by the imprinting process are compressed by a rigid flat platen. A sketch of the model is shown in figure 5. It is noted that the compression depth u is taken to be zero at the original film surface height (before imprinting). Therefore, the first contact between rigid platen and surface asperities occurs at negative values of u. After flattening to $u = 0$ the vertical coordinates of all surface points are smaller or equal to $h = 2\,\mu$m. The unit cell on which the boundary conditions are prescribed has the same width w used for the imprinting simulations.

3.1. Contact between rough surface and rigid platen

It is recalled that imprinting was performed under sticking contact conditions. This was done to maximize the surface roughness: the constraint on unit cell expansion during imprinting is such that part of the material is squeezed upward to create material pile-ups around the indenter. Compression is performed here for the same sticking contact conditions, but also when assuming frictionless contact between rough surface and platen. These opposite limiting conditions are chosen because of the lack of an appropriate model for the real friction conditions between the two bodies; the real behavior is expected to be in between the limiting cases treated.

To model sticking and frictionless contacts, respectively, the following boundary conditions are prescribed at the points of contact S_u between the rough surface $h(x_1)$ and the rigid flat indenter:

$$\begin{array}{lll} \text{(a) perfect sticking :} & u_1(x_1, h(x_1)) = 0, & u_2(x_1, h(x_1)) = -\int \dot{u}\,\mathrm{d}t; \\ \text{(b) frictionless :} & \sigma_{12}(x_1, h(x_1)) = 0, & u_2(x_1, h(x_1)) = -\int \dot{u}\,\mathrm{d}t. \end{array} \tag{9}$$

The periodic boundary conditions when the contact is sticking can remain as in (6) but need to be changed when the contact is frictionless, since then the material can expand freely in the lateral (x_1)-direction. With reference to [15] for details, the periodicity conditions for frictionless contacts are

$$u_1(w, x_2) - u_1(0, x_2) = U_1 \qquad u_2(0, x_2) = u_2(w, x_2) \tag{10}$$

where the value of the uniform expansion U_1 is determined from the condition that lateral expansion takes place freely,

$$\frac{1}{h}\int_0^h \sigma_{11}(x_1, x_2)\,\mathrm{d}x_2 = 0 \qquad \forall x_1. \tag{11}$$

3.2. Effect of contact conditions on flattening

A thin film that was previously imprinted by a template with $w = 2\,\mu$m is flattened here by a rigid platen to $u = 0.05\,\mu$m, unloaded and relaxed. The contrast in response under sticking versus frictionless contact is shown in figure 6. As shown in figure 6(*a*), the compression force for perfect sticking boundary conditions rises steeply to about $4000\,\mu\mathrm{N}\,\mu\mathrm{m}^{-1}$ at maximum compression. The contact area increases rapidly under sticking contact such that at $u = 0.02\,\mu$m the contact is almost complete, as shown in figure 6(*b*). Together with the fact that the unit cell cannot expand, a high hydrostatic pressure state is generated inside the film, which leads to the slope of the force response being close to the elastic solution. By contrast, under frictionless contact, lateral expansion allows the entire film to yield. As a consequence the contact force remains much lower (less than $300\,\mu\mathrm{N}\,\mu\mathrm{m}^{-1}$), resulting in a maximum contact length of only about $0.4w$.

The effect of contact conditions on the efficiency of flattening can also be seen in figure 7(*a*), which shows the profile of the initial rough surface before compression, at maximum compression depth and in the final, unloaded and relaxed state. The top surface compressed with perfect sticking contact is much flatter than with frictionless contacts. The sticking rigid platen is more effective in flattening out the surface asperities, figure 7(*b*), although it requires a very high load. Also note that under these conditions, the average thickness is close to the pristine value of $h = 2\,\mu$m, while permanent thinning of the film has occurred when flattened under frictionless conditions due to yield of the entire film. Figure 8 shows the evolution of the roughness R_m for sticking and frictionless contact as well as the height–height correlation function $H_\mathrm{r}(r)$. While the roughness decreases significantly during compression when the contact is sticking, it decreases much less when the contact is

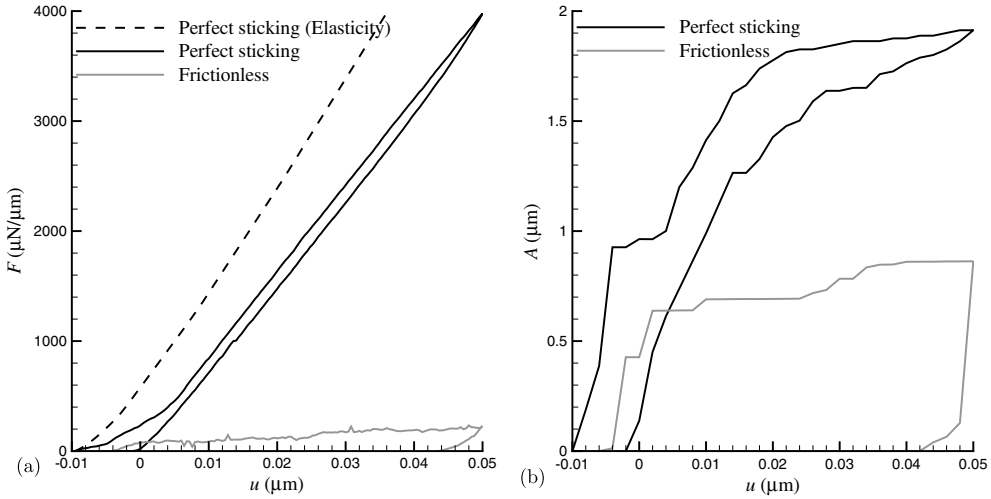

Figure 6. (*a*) Force response and (*b*) evolution of contact area A during compression of a previously imprinted film with $w = 2\,\mu$m under either perfect sticking or frictionless contact.

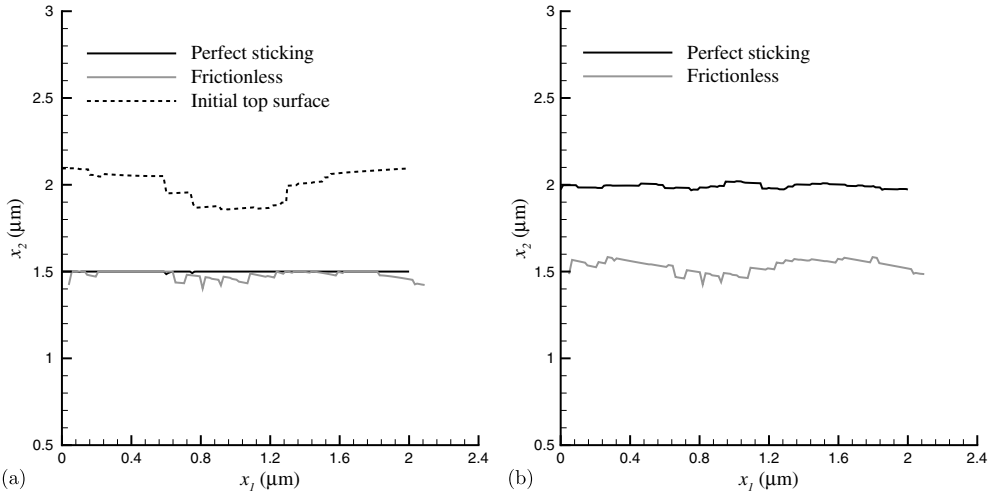

Figure 7. Profile of top surface of the films reported in figure 6 for different boundary conditions (*a*) at maximum compression depth $u = 0.05\,\mu$m; (*b*) after unloading and relaxation. The vertical displacement is magnified by a factor 10.

frictionless. Since the contact area achieved under sticking contact at the maximum imprinting depth is larger, $A = 1.93\,\mu$m, than that achieved under frictionless contact, $A = 0.86\,\mu$m, we perform an additional simulation under sticking contact to also achieve a maximum contact area of $A = 0.86\,\mu$m. The corresponding height–height correlation function is included in figure 8(*b*). Results show that if the same contact area is achieved, i.e. for a similar flattening of the asperities, the contact conditions are not so critical in determining the roughness after unloading: $R_{\mathrm{m}} = 3.93 \times 10^{-3}\,\mu$m for sticking and $R_{\mathrm{m}} = 3.56 \times 10^{-3}\,\mu$m for frictionless compression. Moreover, the height–height correlation functions are closer, but have a different shape. Thus, the contact conditions affect surface evolution and topography rather significantly.

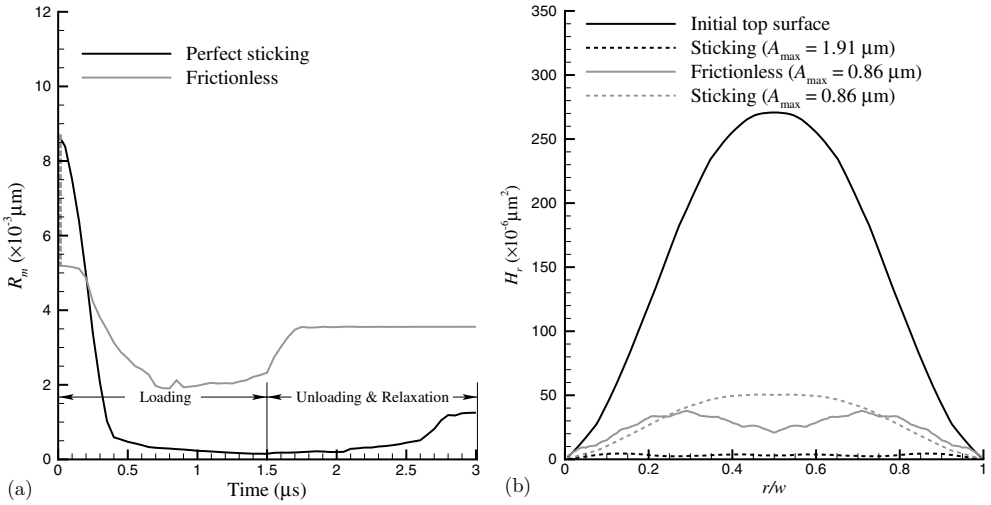

Figure 8. (*a*) The evolution of surface roughness R_{m} during compression under sticking and frictionless contacts. (*b*) $H_{\mathrm{r}}(r)$ after unloading and relaxation, corresponding to figure 7. The film was previously imprinted with $w = 2\,\mu$m to $u_{\max} = 0.05\,\mu$m.

With reference to figure 7 it is noteworthy that for either contact condition the topography of the final surface profiles does not show any resemblance to the original surface profiles.

3.3. Effect of loading history

The initial condition for the film studied in the previous section was equal to the final state immediately after it had been imprinted. This means that it contained the dislocations and the residual stress due to previous imprinting. This initial state could assist the flattening process, but might also obstruct it. To investigate this, we study the compression of all films imprinted in section 2.2 and contrast them with results obtained by compressing films with the same surface profiles but cleared of initial dislocations and residual stresses. Experimentally, this might be done, at least partly, by a heat treatment. We again consider the limiting cases of sticking and frictionless contacts.

3.3.1. Flattening of the surface by a sticking platen. For the case of sticking contact we will limit the maximum compression depth to $u_{\max} = 0.01\,\mu$m to avoid the regime where unrealistic high stresses build up and the rough surface gets squashed flat completely, as was observed in figure 6. Figure 9 shows the evolution of compression force and contact area for the films. The films without initial dislocations and stresses consistently need a larger force to be flattened by the sticking contact. A clear trend cannot be seen in the development of contact area, i.e. the contact area for films that start dislocation- and stress-free does not systematically develop a smaller or larger real contact area with the platen. On the other hand, the evolution of surface roughness R_{m} (figure 10(*a*)) shows a connection between the presence of initial dislocations and roughness: all films that started dislocation- and stress-free are less flattened by the compression and develop a larger roughness during unloading and relaxation. It appears therefore that the presence of dislocation and stresses favors the squeezing of the asperities. The height–height correlation functions in figure 10(*b*) reveal lower and broader peaks for the flattened films compared with the imprinted films (see figure 4(*b*)) for all starting conditions.

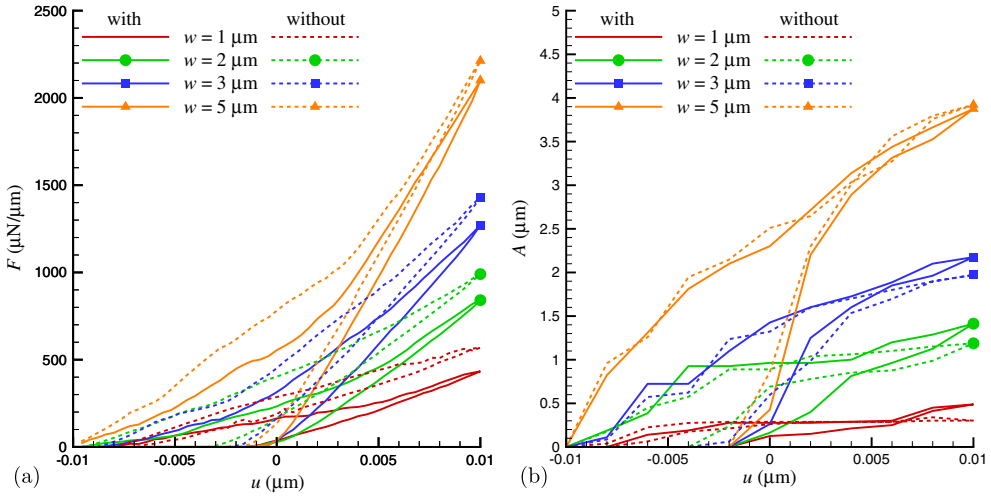

Figure 9. The evolution of (*a*) compression force F and (*b*) contact area A with u for sticking boundary contact between platen and rough surface in the presence of the residual dislocations and stresses (labeled 'with') and after their removal (labeled 'without').

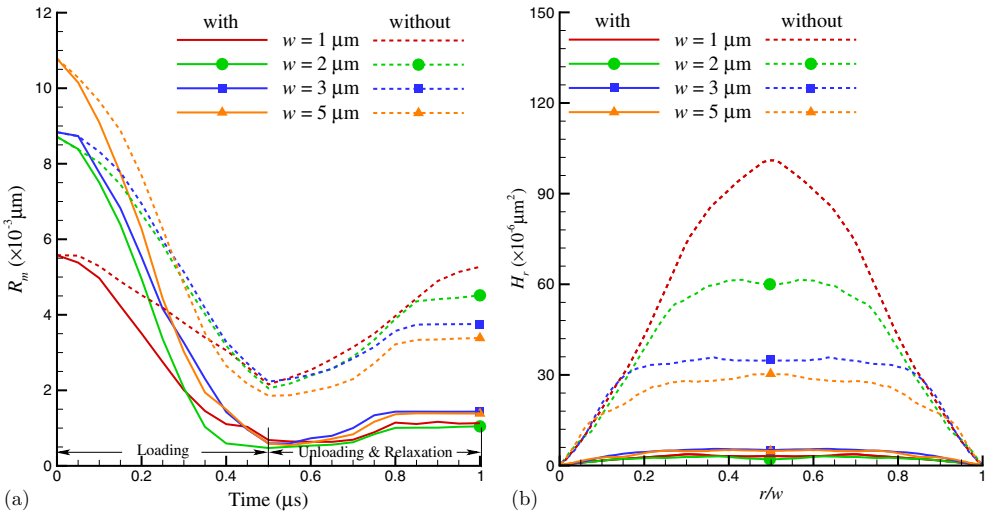

Figure 10. The evolution of (*a*) roughness R_{m} with compression time for different widths under perfect sticking contact. (*b*) Height–height correlation functions at the end of the process.

Broader peaks correspond to a more homogeneous surface roughness, which together with a lower value of R_{m} means a more flattened surface.

It is noteworthy that the films with the dislocations retained after imprinting have a more homogeneous surface roughness; this indicates that the flattening of the surface has been aided by the presence of dislocations. This can be better seen in figure 11, which shows the surface profiles obtained after flattening one of the films, namely the $w = 3\,\mu$m film. The case without initial dislocations resembles the as-imprinted profile more than the case with initial dislocations. For the same film the dislocation structure before and after compression

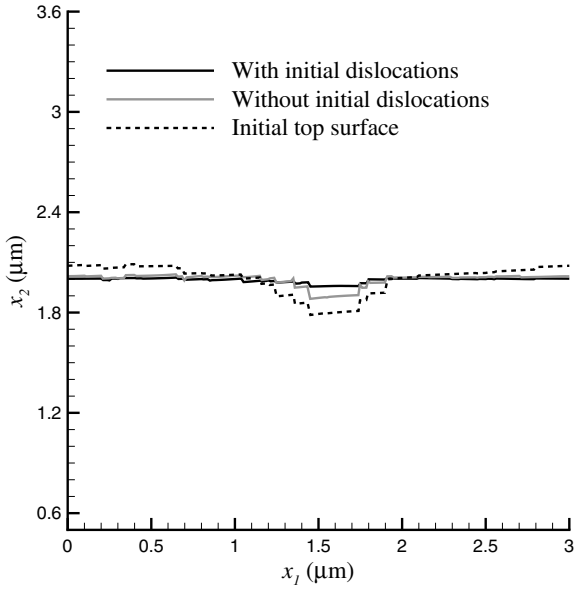

Figure 11. Surface profiles after compression under sticking contact conditions of the film with $w = 3\,\mu$m.

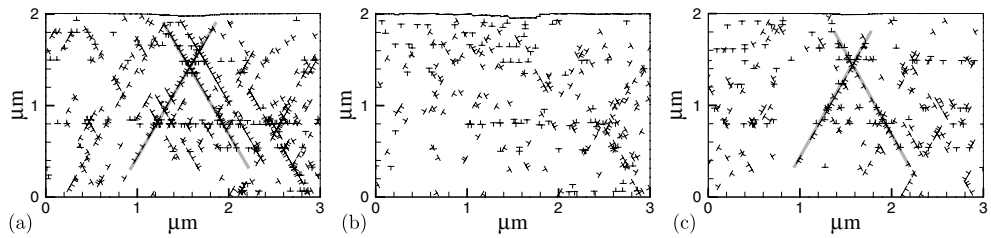

Figure 12. Dislocation structure in the film $w = 3\,\mu$m (*a*) before and after compression for the case (*b*) with and (*c*) without initial dislocations.

is shown in figure 12. The dislocation structure in figure 12(*b*), which represents the film compressed from the film in figure 12(*a*), shows little resemblance with the structure in the original as-imprinted film. During compression, the retained dislocations have left the free surface and facilitated the squeezing of the imprint. On the other hand the flattening of the film without initial dislocations in figure 12(*c*) has been more difficult; at the beginning of compression dislocations were not available to glide and by that help flattening the imprint. Only at a later stage of compression dislocations have been nucleated in the film in relation to the stress singularity at the corners of the imprint (these dislocations are indicated by the lines in figure 12(*c*)). The evolution of the dislocation density during compression for all the films analyzed can be seen in figure 13. The films with retained dislocations obviously start from a higher dislocation density, but this decreases almost monotonically during compression, unloading and relaxation. Initially dislocation-free films, however, accumulate dislocation density during compression and reach a similar density at the end of the process.

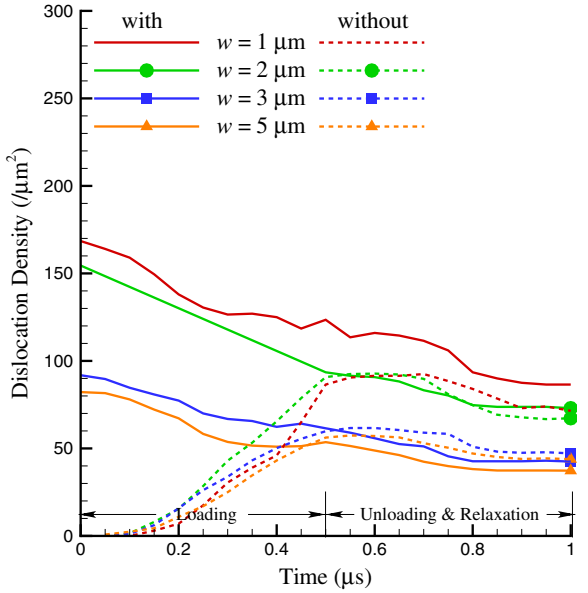

Figure 13. Evolution of the dislocation density in films with and without initial dislocations under sticking contact for various initial surface profiles.

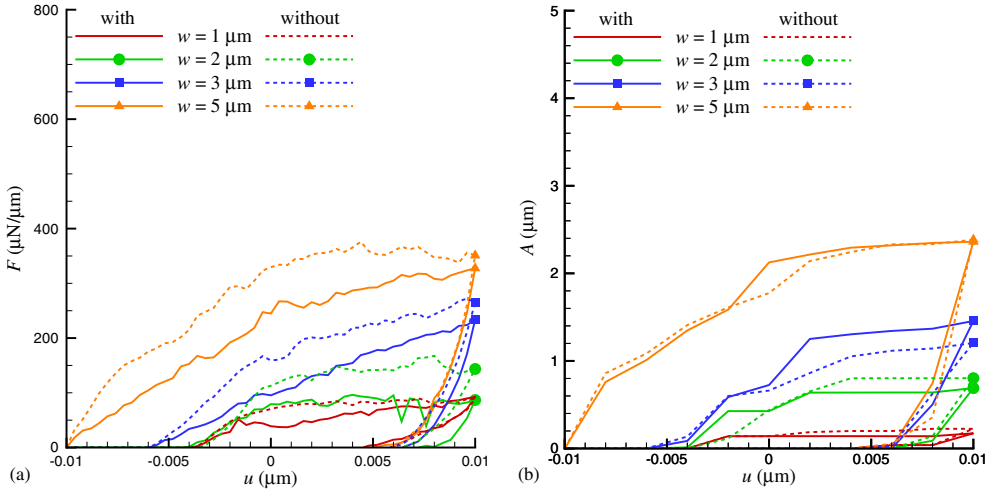

Figure 14. The evolution of (*a*) compression force F; (*b*) contact area A with compression depth u for different widths under frictionless contact. The maximum indentation depth is $u = 0.01\ \mu$m.

3.3.2. Flattening rough surfaces by a frictionless platen. The imprinted films are also compressed without friction (to the same $u = 0.01\,\mu$m). The corresponding force–displacement curves and contact area evolution are shown in figure 14. Films with the same profile but different histories—i.e. with or without initial dislocations and stresses—exhibit different force–displacement curves, i.e. the presence of initial dislocations gives rise to a softer response. A similar trend cannot be seen in the evolution of the contact area, which appears to

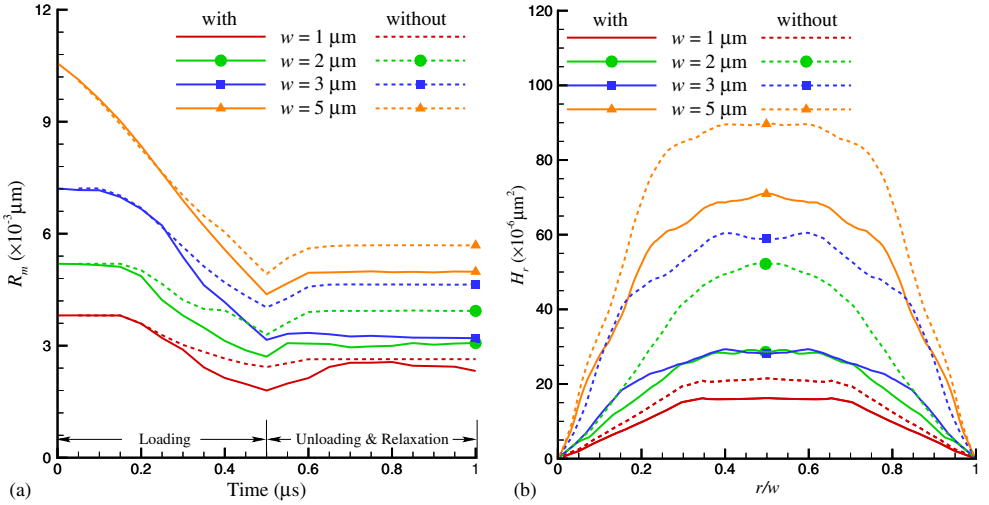

Figure 15. (*a*) Roughness evolution with frictionless compression of pre-imprinted films with and without initial dislocations. (*b*) $H_r(r)$ after unloading and relaxation ($t = 3\,\mu$s). The maximum indentation depth is $u = 0.01\,\mu$m.

depend on starting conditions but without a clear tendency. These observations are qualitatively similar to those made in the previous subsection on sticking contacts. Also consistent with the results obtained with sticking conditions, the change in roughness R_m during compression and the height–height correlation functions at the end of the process, presented in figure 15, show that for each film the flattening process is facilitated by the presence of dislocations retained by the imprinting process. Differently from the cases with sticking contact, though, all films with retained dislocations are not flatter than the initially dislocation-free films. Moreover, the difference in roughness between the films with and without retained dislocations is lower than for the sticking contact. A smaller influence of the loading history can be seen also by contrasting the final profiles for the film with $w = 3\,\mu$m, figure 16(*a*), with those for the same films under sticking compression in figure 11. The dislocation density in figure 16(*b*) for the films with retained dislocations decreases less during the process than that for the sticking contact in figure 13. All the observations lead to the conclusion that the presence of retained dislocations aids the flattening of asperities compressed under all friction conditions, but the effect is smaller if there is no friction.

The situation changes slightly when the films are flattened to a larger compression depth, i.e. $u = 0.05\,\mu$m. Both the change in roughness R_m during compression and the height–height correlation functions at the end of the process, presented in figure 17, have lost their dependence on the presence or absence of initial dislocations. For all films, the final surface roughness is rather homogeneous, as indicated by the broad height–height correlation functions. Thus, under frictionless contact the presence of initial dislocations does facilitate flattening of the surface only at smaller compression depths, when the contact area is about one third of the surface area. When the contact area becomes larger, the film is subjected to a uniform compression which leads to yielding of the metal and a much higher and less localized dislocation activity. Consequently, the dislocation density peaks at maximum compression depth, as seen in figure 18. This is consistent with the observation in figure 6 that with these contact conditions, the film can yield as a whole.

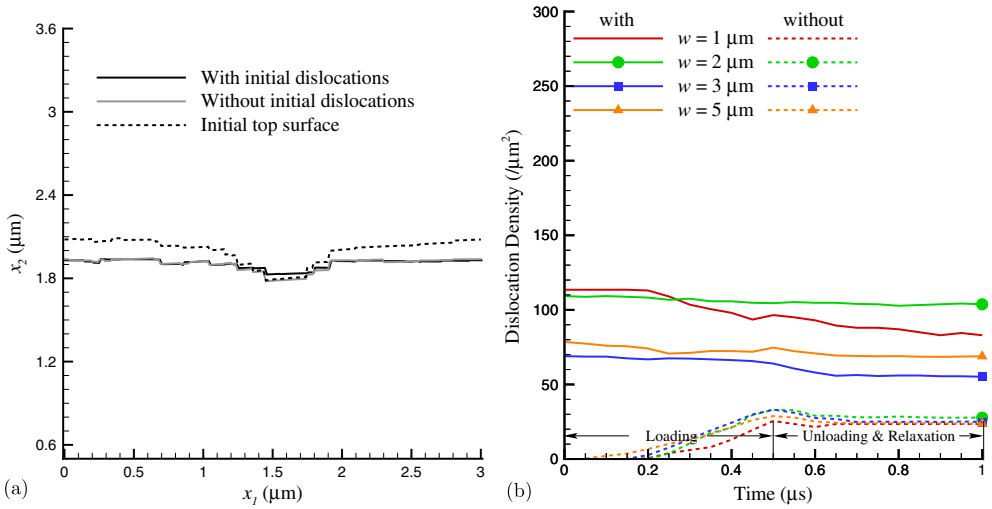

Figure 16. (*a*) Final profiles for the $w = 3\ \mu$m film and (*b*) evolution of dislocation density during compression and relaxation of films flattened by a frictionless contact to $u = 0.01\ \mu$m.

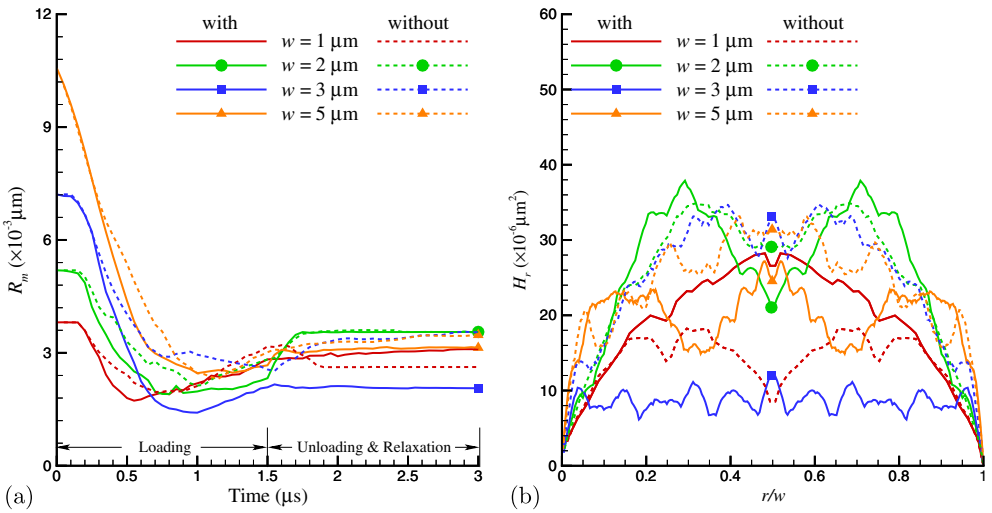

Figure 17. (*a*) Roughness evolution with frictionless compression down to $u = 0.05\ \mu$m of pre-imprinted films with and without initial dislocations. (*b*) $H_r(r)$ after unloading and relaxation ($t = 3\ \mu$s).

The reader is reminded here that in the simulations dislocation nucleation occurred from Frank–Read sources and that nucleation of dislocations from surface steps was not considered. Also, geometry changes were not accounted for other than in the evolution of the contact area. It is foreseeable that if the model would be improved by including geometry changes and dislocation nucleation from the surface, a larger density of glide planes would be activated and the final surface profile would be smoother. This is expected especially in the case of frictionless contact. However, the effect of retained dislocations gliding and aiding the flattening is not expected to be reduced.

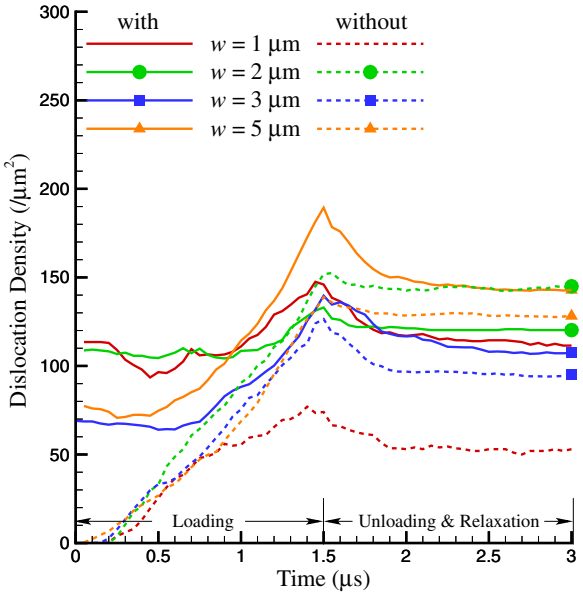

Figure 18. Evolution of dislocation density during compression and relaxation of films flattened by a frictionless contact down to $u = 0.05\,\mu$m.

4. Conclusions

We have performed discrete dislocation plasticity simulations of the flattening of surface roughness obtained by nanoimprinting thin metal films. The imprinting simulations have shown that the imprints are much wider than the indenters that produced them. The shape of the indents is determined primarily by the density of dislocation sources. The metal surface in between imprints is also affected by the dislocation activity, namely through dislocations that exit the metal thus leaving rather pronounced displacement steps at the surface. Also, the interaction between neighboring plastic zones contributes to the final roughness of the surface. Specifically, surfaces indented by contacts that are closer than the material dependent length of $w \approx 7\,\mu$m exhibit squeezing-up of material in the region between neighboring indents. In other words, the shape of the final surface resembles a wave that has the same periodicity of the spacing between indenters w.

Flattening of the films has been achieved by compressing the rough surface obtained by nanoimprinting using both frictionless and sticking contact conditions. The results differ quite significantly when the surfaces are flattened to the same depth (which corresponds to a rather different contact area): the sticking contact leads to a more pronounced flattening of the surface asperities, albeit at a much higher contact pressure.

The focus of this study has been on contrasting the behavior of the as-imprinted film surfaces—with stresses and dislocations produced by the nanoimprinting process—with those of films with the same surface profiles but freed of dislocations and stresses. For both sticking and frictionless contact, and for compression depths that cause only partial flattening of the surface, the evolution of the surface topography depends strongly on the loading history, i.e. the presence or absence of dislocations retained during imprinting. More precisely, the presence of initial dislocation favors the squeezing of asperities. This observation is obviously not sufficient to claim that the presence of dislocations in the subsurface region favors flattening of the

asperities in general, since the dislocation structure created during imprinting is characteristic of this specific deformation process only. On the other hand it can be concluded that the loading history strongly affects the deformation of the surface profile during contact. This indicates that an accurate description of the surface profile is not sufficient to predict initial deformation of the surface during contact of rough surfaces, independently of friction conditions. Therefore, models that aim at predicting rough surface evolution should not only strive to a precise description of the rough surface, but also acquire a similarly accurate knowledge of subsurface dislocation structure.

Acknowledgments

LN is grateful to the Dutch National Scientific Foundation NWO and Dutch Technology Foundation STW for their financial support (VENI grant 08120).

References

[1] Greenwood J A and Williamson J B P 1966 Contact of nominally flat surfaces *Proc. R. Soc. Lond. Ser.* A **295** 300–19
[2] Jackson R L and Green I 2006 A statistical model of elasto-plastic asperity contact between rough surfaces *Tribol. Int.* **39** 906–14
[3] Gao Y-F and Bower A F 2006 Elastic–plastic contact of a rough surface with Weierstrass profile *Proc. R. Soc. Lond. Ser.* A **462** 319–48
[4] Majumdar A and Bhushan B 1991 Fractal model of elastic–plastic contact between rough surfaces *J. Tribol.* **113** 1–11
[5] Ciavarella M, Delfine G and Demelio G 2006 A revitalized Greenwood and Williamson model of elastic contact between fractal surfaces *J. Mech. Phys. Solids* **54** 2569–91
[6] Yan W and Komvopoulos K 1998 Contact analysis of elastic–plastic fractal surfaces *J. Appl. Phys.* **84** 3617–24
[7] Wilson W E, Angadi S W and Jackson R L 2009 Surface separation and contact resistance considering sinusoidal elastic–plastic multi-scale rough surface contact *Wear* **268** 190–201
[8] Patir N 1978 A numerical procedure for random generation of rough surfaces *Wear* **47** 263–77
[9] Bakolas V 2003 Numerical generation of arbitrarily oriented non-Gaussian three-dimensional rough surfaces *Wear* **254** 546–54
[10] Wu J J 2000 Simulation of rough surfaces with FFT *Tribol. Int.* **33** 47–58
[11] Van der Giessen E and Needleman A 1995 Discrete dislocation plasticity: a simple planar model *Modelling Simul. Mater. Sci. Eng.* **3** 689–735
[12] Rice J R 1987 Tensile crack tip fields in elastic-ideally plastic crystals *Mech. Mater.* **6** 317–23
[13] Nicola L, Van der Giessen E and Needleman A 2004 Relaxation of thermal stress by dislocation motion in passivated metal interconnects *J. Mater. Res.* **19** 1216–26
[14] Nicola L, Bower A F, Kim K S, Needleman A and Van der Giessen E 2008 Multi-asperity contact: a comparison between discrete dislocation and crystal plasticity predictions *Phil. Mag.* **88** 3713–29
[15] Nicola L, Bower A F, Kim K S, Needleman A and Van der Giessen E 2007 Surface versus bulk nucleation of dislocations during contact *J. Mech. Phys. Solids* **55** 1120–44